PAPER

Check for updates

A study of plant growth regulators detection based on terahertz time-domain spectroscopy and density functional theory

Xiaoxue Du, [ID] [ab] Yafei Wang,[ab] Xiaodong Zhang,[ab] Guoxin Ma,[ab] Yong Liu,[ab] Bin Wang[ab] and Hanping Mao*[ab]

Terahertz technology is receiving increasing attention for its use as an efficient non-destructive, non-contact and label-free optical method for qualitative and quantitative detection. The aim of this study was to develop a chemical analysis methodology based on terahertz time-domain spectra that could be used to detect plant growth regulators, such as glyphosine, naphthaleneacetic acid, daminozide and gibberellic acid. The THz fingerprint spectra of these four PGRs were located in the 0.3–1.8 THz, with the peaks of glyphosine at 0.32, 0.49, 0.74, 0.87, 0.96, and 1.49 THz; daminozide at 0.33, 0.39, 0.55, 0.67, and 1.17 THz; gibberellic acid at 0.46, 0.58, 0.92, and 1.38 THz and naphthaleneacetic acid at 0.43, 0.57, 0.73, and 0.90 THz. The results showed that these four plant growth regulators exhibited numerous distinct spectral features in frequency-dependent absorption spectra, which demonstrated the qualitative capacity of terahertz time-domain. The origin of the observed terahertz absorption peaks of these four plant growth regulators was determined through density functional theory calculations and analysis of absorption spectra. Discriminant analysis method was used to evaluate the classification trends of the four plant growth regulators based on their THz absorbance spectra. Generally, this study provides a reference for the rapid detection of plant growth regulators in fruits and vegetables by using terahertz spectroscopy technology.

1. Introduction

Plant growth regulators (PGRs) are natural hormones and synthetic hormone analogs that can be used to regulate the physiology and metabolism of crops. They have been widely used in fruit production to increase yield and improve quality.[1–3] At low concentrations, PGRs can affect cell division, cell expansion, and cell structure and function, as well as mediate environmental stress.[4] Although PGRs are often applied to agricultural plants, the excessive application of PGRs can cause fruits and vegetables to retain PGR residues, which are potentially toxic to humans.[5] Thus, the excessive use of PGRs poses a threat to public health, as their toxic effects can lead to digestive and endocrine disorders, chronic kidney diseases, cancer, and other diseases.[6–9] Several legislative bodies, including the European Union, the United States, Japan, and China, have established maximum residue limits for PGRs. However, some PGRs are difficult to monitor and detect. There is thus a need to develop reliable techniques for the rapid and sensitive detection of these residues to ensure food safety.

Several advances have been made in the detection and identification of PGRs over the past decades using conventional analytical methods, such as thin-layer chromatography, capillary electrophoresis, gas chromatography, high-performance liquid chromatography, enzyme-linked immunosorbent assays, and immune-affinity column assays.[10–13] However, these methods are time-consuming and require complex sample pretreatment steps. Thus, enhanced purification techniques are needed for multiclass PGR analysis given the low concentrations of PGRs and the complexity of their matrices.

The terahertz frequency of the electromagnetic spectrum lies between the infrared band and the microwave band and ranges in frequency from 0.1 to 10 THz (wavelength between 3 mm–30 μm). Because of its non-ionization, low energy, high sensitivity, and fingerprint spectroscopy of THz waves, THz spectroscopy has become a useful technique for qualitative and quantitative detection. THz spectroscopy has been used in chemistry, biology, medical science, homeland security, and food safety.[14–18] Haddad *et al.* (2014) used chemometrics to analyze ternary mixtures of fructose, lactose, and citric acid with transmission terahertz time-domain spectroscopy (THz-TDS). They found that principal component analysis (PCA) could be used effectively to analyze THz data of ternary mixtures.[19] Xie *et al.* (2019) used THz-TDS to detect tetracycline hydrochloride and its degradation products over the temperature range of 4.5–

aSchool of Agricultural Engineering, Jiangsu University, Zhenjiang, PR China. E-mail: dx666140474@163.com

bKey Laboratory of Modern Agricultural Equipment and Technology, Ministry of Education, Jiangsu University, Zhenjiang, PR China. E-mail: maohpujs@163.com

300 K. Density functional theory (DFT) calculations and analysis of temperature-dependent absorption spectra could effectively resolve the origin of the observed THz absorption peaks of four tetracyclines.[20] Furthermore, DFT has been shown to be an effective theoretical method for accurately predicting vibrational frequencies for medium-size molecules. The combined use of both THz-TDS and DFT has been shown to be effective for determining the characteristic spectra of illegal drugs.[21]

In this study, we show that THz-TDS is an effective method for detecting PGRs, such as glyphosine, naphthaleneacetic acid, daminozide, and gibberellic acid, and use DFT to analyze the source of each absorption peak. Generally, this approach could be used for the high-performance analysis of biological and chemical molecules. We also conducted analyses to distinguish the vibrational modes from intermolecular vibration modes and phonon modes. Compared with PCA, the discriminant analysis (DA) method shows a more obvious tendency to classify the terahertz absorption spectra of the four PGRs.

2. Experimental

2.1 Sample preparation

Glyphosine (>97%, BR), naphthaleneacetic acid (>98%, BR), daminozide (>99%, BR), and gibberellic acid (>99%, BR) were purchased from Dalian Meilum Biotechnology Co., Ltd. and used without further purification. All samples were gently ground using a mortar and pestle and were then pressed into circular disks with a tablet machine (Tianjin Tianguang Optical Instrument Co., Ltd., China) under 12 MPa of pressure for 2 min. The sample thickness was about 1.5 mm, and the diameter was approximately 6 mm. Several procedures were conducted to address the unevenness and adhesion during tablet pressing. First, a small amount of polyethylene powder was spread flat on the bottom of the tablet mold. Next, the pure sample powder was placed on the polyethylene powder and made flat; a small amount of polyethylene powder was then placed on the top of the sample powder, and the tablet was pressed. To minimize the effect of the inhomogeneity of the sample distribution on the experimental results, the samples were placed for at least half an hour in advance so that the shape and size of the presser would not change. Each sample was measured three times, rotated in 120° increments.

2.2 Experimental apparatus

We used a standard THz-TDS imaging system (TAS7400SP, Advantest INC, Japan) to study the optical properties of PGRs. Experiments were conducted using the transmission mode (Fig. 1). The function of the sample support part of the transmission module is dry air purification. During the detection process, the moist air can be discharged through high-purity nitrogen to prevent the water in the air from affecting the experimental results. In this study, the THz region for sample detection was in the range of 0.3–2.5 THz with a frequency resolution of 1.9 GHz. Air was used as the reference and detected under the same detection conditions. All
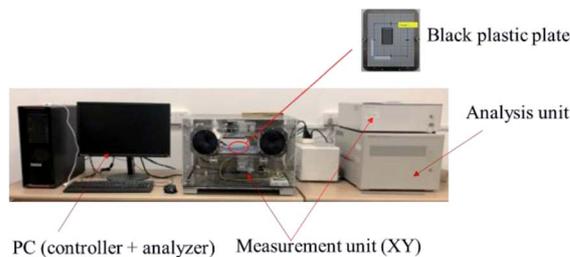

Fig. 1 Terahertz time-domain spectral imaging system.

measurements are performed in a nitrogen atmosphere at a temperature of 25 °C (±1 °C) and a relative humidity of less than 3%.

2.3 Data analysis

Glyphosine, naphthaleneacetic acid, daminozide, and gibberellic acid samples were measured using the THz-TDS system. Based on the optical parameter extraction procedure of Dorney and Duvillaret *et al.*,[22,23] reference spectra $E_{ref}(w)$ and sample spectra $E_{sam}(w)$ were obtained by scanning background and samples, respectively. By calculating the ratio $T(w)$ of the frequency domain spectrum of $E_{sam}(w)$ and $E_{ref}(w)$, the complex refractive index and extinction coefficient of the sample can be obtained; the absorption spectra of the samples can then be obtained. The normal incidence was used in experimental measurements; the incidence angle and refraction angle were both 0, and the multiple reflections of the THz wave in the sample were ignored. The formula for calculating the electric field of the THz wave was as follows:

$$E_{out}(w) = E_{in}(w) \times T(w) \times P_{sam}(w) \times P_{air}(w) \quad (1)$$

where $E_{in}(w)$ and $E_{out}(w)$ are the incident electric field and the outgoing radio field, respectively; $T(w)$ is the transmittance; $P_{air}(w)$ and $P_{sam}(w)$ are the transmission factors of THz waves in the air and samples, respectively; and the transmittance $T(w)$ is as follows:

$$T(w) = \frac{E_{out}(w)/P_{sam}(w)}{E_{in}(w) \times P_{air}(w)} = \frac{E_{sam}(w)}{E_{ref}(w)} \quad (2)$$

By applying the fast Fourier transform, we obtained the corresponding frequency-domain sample and reference THz spectra, which were denoted as $E_{sam}(w)$ and $E_{ref}(w)$, respectively. The THz absorbance spectra of all samples can then be obtained according to the following formula:[24]

$$Absorbance(w) = -\log\left|\frac{E_{sam}(w)}{E_{ref}(w)}\right|^2 \quad (3)$$

2.4 DFT analysis

DFT uses the electron density distribution as the basic variable to study the ground state properties of multi-particle systems. DFT is a computational quantum mechanical modeling method that has been used in the fields of chemistry, physics, and

materials science to study the electronic structure of multi-electron systems.[25–27] This method has also become a standard computational tool for analyzing molecular vibrational modes in the electromagnetic spectrum, including the THz region.[28,29] To understand the observed THz absorption features from molecular structures, isolated molecule ground state geometry optimization and frequency calculations were performed using Gaussian 09 software. DFT calculations with B3LYP/3-21G(*) were then conducted to assign the vibrations of the four PGRs.[30] To obtain realistic vibrational properties of four PGRs, firstly, the structure of PGRs based on the experimental infrared spectra from the Shanghai Objective Database (http://www.basechem.org/) was used to provide the initial gas-phase single-molecule geometry, and then molecular geometry was fully optimized and the harmonic vibration frequency calculation was performed. Finally, minimum energy structures were found, which were confirmed by vibrational analyses. Furthermore, the calculated results were analyzed to ensure no imaginary frequency was found. The single molecular structures of glyphosine, naphthaleneacetic acid, daminozide, and gibberellic acid predicted after the geometry optimization are shown in Fig. 2(a)–(d), respectively.

3. Results and discussion

3.1 THz spectra of PGRs based on DFT theory

Vibrations of molecules in the THz frequency region mainly stem from the deformation vibration, bending vibration, and distortion produced by collective vibrational modes.[25,31] Different vibrations lead to variation in the position of peaks. Because the effect of electron correlation and the non-harmonic effect were ignored in the DFT simulations, a frequency correction factor of 0.96 was used to modify the frequency for the method and basis set.[32] The epsilon represents the molar absorption coefficient. The experimental and simulated THz absorbance spectra of glyphosine, naphthaleneacetic acid, daminozide, and gibberellic acid in the range of 0.3–2.0 THz are shown in Fig. 3(a)–(d), respectively. Because the vibrational modes of the isolated-molecule simulation are often characterized as the bending, twisting, and deformation of the atoms, we analyzed the origin of the THz absorption peaks of PGRs. The experimental and calculated vibrational frequencies of absorption peaks, as well as the assignments of these vibrational modes, are summarized in Table 1. Fig. 4(a)–(d) show the displacement vector representations of the THz
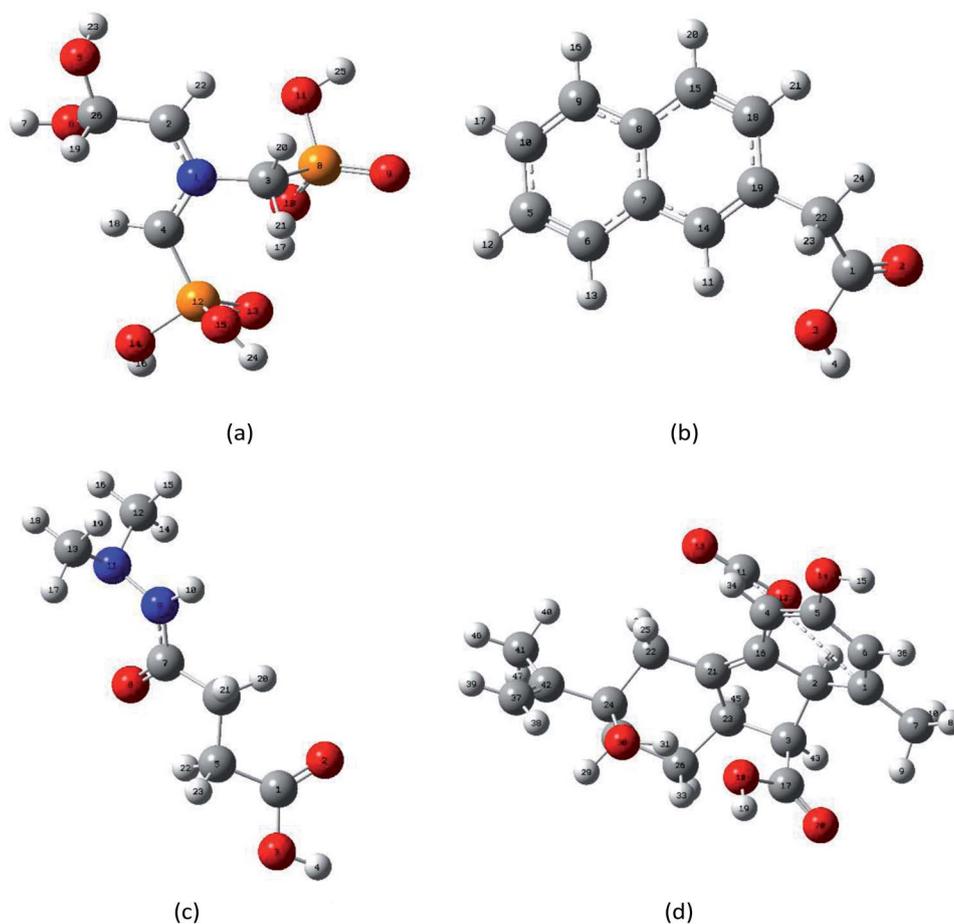

Fig. 2 Optimized geometrical structures of isolated-molecules using DFT calculations: (a) glyphosine, (b) naphthaleneacetic acid, (c) daminozide, (d) gibberellic acid.
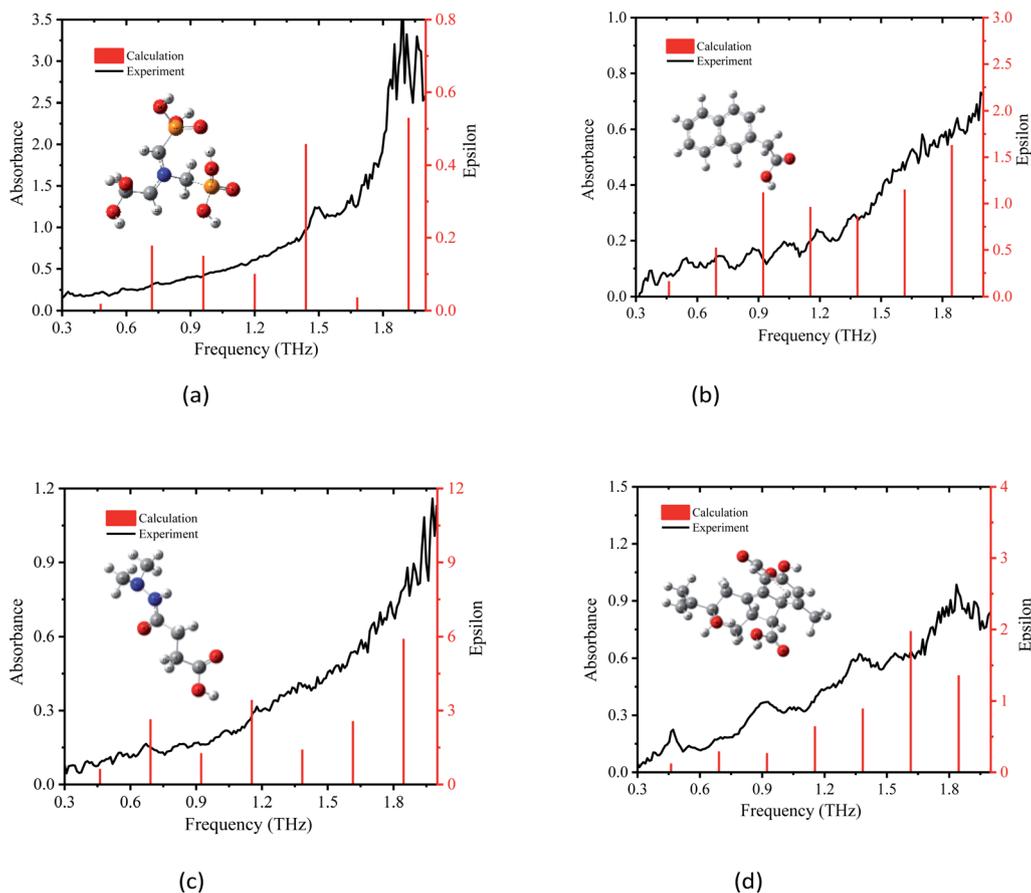
Fig. 3 Comparison of absorption spectrum of PGRs between experiment and Gaussian calculation, (a) glyphosine, (b) naphthaleneacetic acid, (c) daminozide and (d) gibberellic acid.

vibrational modes of glyphosine at 0.49 and 0.96 THz, naphthaleneacetic acid at 0.71 and 1.04 THz, daminozide at 0.67 and 1.17 THz, and gibberellic acid at 0.46, 0.92, and 1.38 THz, respectively; the arrowheads represent the displacement vectors.

The simulated absorbance peak at 1.49 THz for glyphosine is consistent with pure glyphosine in the presence of poly-ethylene powder (Fig. 3(a)), which indicated that the peak at 1.49 THz represents the characteristic absorption peak of glyphosine. The experimental absorption peak of glyphosine at 1.49 THz was attributed to the calculated intramolecular vibrational mode at 1.44 THz, which was mainly caused by the C3–P8–C11 wagging vibration out of the plane. In addition, some other absorption peaks were detected, such as the peaks at 0.49, 0.74, and 0.96 THz, which were mainly caused by the H7–O6–C25–H19 rocking vibration in the plane, O9–P8–O10 wagging vibration out of the plane, and H23–O5–C26–O6 wagging vibration out of the plane, respectively. The other experimental absorption peaks of glyphosine at 0.32 and 0.87 THz, which were absent in the DFT calculations, may stem from the intermolecular vibrational modes or phono modes. Experimental and simulation results show that DFT can reflect the vibration of molecules. We also obtained experimental and calculated vibration frequencies for

the absorption peaks of the other three PGRs, as well as the assignments and sources of these vibrational modes. It is also worth noting that the theoretical data from DFT was still slightly differed to assign vibrational modes to all peaks in the experimental spectra due to the lack of intermolecular forces.[20]

The experimental absorption peak of naphthaleneacetic acid at 0.71 THz was attributed to the calculated intramolecular vibrational mode at 0.72 THz (Fig. 3(b)), which was mainly caused by the H23–C22–H24 wagging vibration out of the plane. The vibrational mode at 1.04 THz was mainly attributed to the H12–C5 wagging vibration and H21–C18 wagging vibration. The other peaks at 0.55, 0.88, 1.04, and 1.36 THz may stem from intermolecular modes or phonon modes. Also, the interaction of the carboxylic acid group on the naphthalene ring is of great importance in determining its structure and vibrational properties. So we can conclude that all these absorption peaks originate from the intermolecular interactions of naphthaleneacetic acid.

The experimental absorption peaks for daminozide were basically consistent with the calculations (Fig. 3c), which indicated that these absorption peaks originated from intramolecular vibrational modes. The vibrational mode at 0.67 THz was mainly attributed to the H20–C6–H21 rocking vibration.

Table 1 Assignment of the vibrational modes for PGRs in the frequency region 0.3–1.8 THz[a]

| Samples | Vibrational frequency (THz) | | Assignment |
	Experiment	Calculation	
Glyphosine	0.32	—	—
	0.49	0.48	ρ(H7–O6–C25–H19)
	0.74	0.72	ω(O9–P8–O10)
	0.87	—	—
	0.96	0.96	ω(H23–O5–C26–O6)
	1.19	1.20	ω(O15–P12–O14–H16)
	1.49	1.44	ω(C3–P8–C11)
Naphthaleneacetic acid	0.42	0.48	ω(C22–C1–O3–H4)
	0.55	—	—
	0.71	0.72	ω(H23–C22–H24)
	0.88	—	—
	1.04	0.96	ρ(H12–C5), ρ(H21–C18)
	1.19	1.2	ω(C19–C22–H24)
	1.36	—	—
Daminozide	0.33	—	—
	0.39	—	—
	0.55	0.46	ω(O8–C7–N9–H10)
	0.67	0.69	ρ(H20–C6–H21),
	0.92	0.92	ω(H22–C5–C6–H21)
	1.17	1.15	ω(H22–C5–H23),
Gibberellic acid	0.46	0.46	ρ(O12–C11–O13)
	0.58	—	—
	0.92	0.92	ρ(O10–C17–O20), ω(H8–C7–H9)
	1.38	1.38	τ(O12–C11–O13), ω(H40–C41–H47)

[a] ρ: rocking (in plane), ω: wagging (out of plane), τ: twisting.

The vibrational mode at 1.17 THz was mainly attributed to the H22–C5–H23 wagging vibration. However, there was a difference between the vibrational mode at 0.33 and 0.39 THz in experimental and theoretical calculations. The deviations can be attributed to the fact that the theoretical calculations were aimed at the isolated molecules in the gaseous phase and the experimental results were aimed at the molecule in the solid state.[33]

All four experimental absorption peaks for gibberellic acid were consistent with the calculations (Fig. 3(d)), which indicated that these absorption peaks originated from intramolecular vibrational modes. The vibrational mode at 0.46 THz was mainly attributed to the O12–C11–O13 wagging vibration. The vibrational mode at 1.38 THz was mainly attributed to the H40–C41–H47 wagging vibration and O12–C11–O13 twisting. Meanwhile, the strong hydrogen bond type of interaction between C–H also had a certain impact on vibration. In addition, we can find that the different vibration forms have different absorption peaks (Table 1). The main reason was that the form of vibration between C–O was different.

Compared with the calculated THz absorbance peaks by DFT with B3LYP/3-21G(*), the presence of unpredicted peaks in the experimental absorbance spectra can be attributed to the difference between the simulation and experimental conditions and the lack of intermolecular forces.[34] The experimental peak positions slightly differed among the four

DFT simulated peak positions. This stems from the fact that the simulation modeled the dynamics of PGRs in the gas phase at zero Kelvin, but the experimental results were obtained based on PGR samples at room temperature.[24] Nevertheless, the combination of THz and DFT models with B3LYP/3-21G(*) was effective for characterizing the fingerprint absorption peaks of glyphosine, naphthaleneacetic acid, daminozide, and gibberellic acid.

3.2 Variation of experimental THz absorbance spectra

The stability of THz absorbance spectra in different matrixes is critically important for the analysis of chemicals. The THz spectra of the PGRs obtained in the experiment are shown in Fig. 5(a). Polyethylene was used as a reference because it has a near-zero absorption coefficient.[34] The THz-TDS spectra show that the spectral lines of the four PGRs exhibit a decrease in amplitude and a temporal delay relative to the reference, which indicates that the samples absorb in the THz band. The optical parameter extraction procedure of Dorney et al.[35] was used to process the experimental data. The THz refractive index spectra (Fig. 5(b)) and absorption coefficient spectra (Fig. 6) of the samples were obtained. Fig. 5(b) shows that the refractive index of the four PGRs was higher than that of polyethylene, and they remained stable in the range of 0.3–1.8 THz. Glyphosine has an inflection point after 1.8 THz, indicating that the signal strength after 1.8 THz, as well as the signal-to-noise ratio, is reduced. There is thus
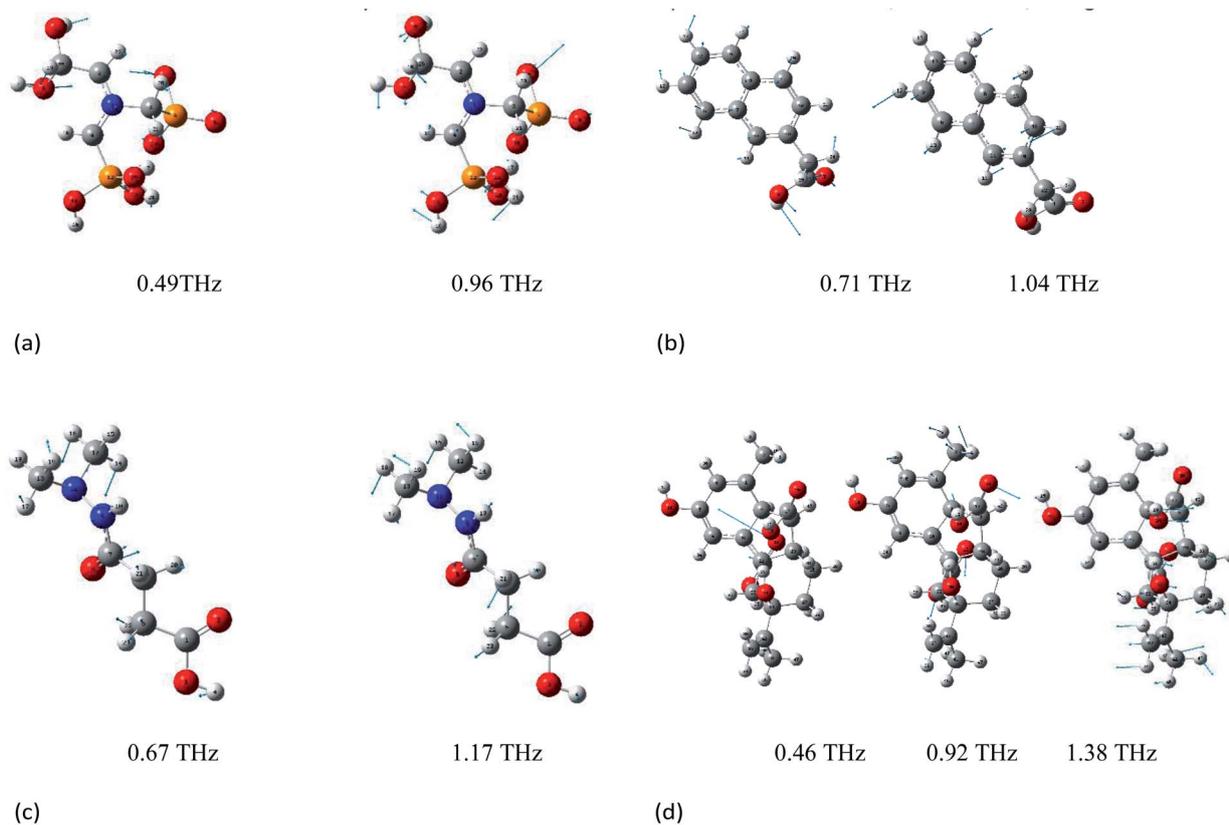
Fig. 4 Displacement vector representation of the vibrational modes of PGRs. (a) Displacement vector representation of the vibrational modes of glyphosine at 0.49 and 0.96 THz. (b) Displacement vector representation of the vibrational modes of naphthaleneacetic acid at 0.71 and 1.04 THz. (c) Displacement vector representation of the vibrational modes of daminozide at 0.67 and 1.17 THz. (d) Displacement vector representation of the vibrational modes of gibberellic acid at 0.96, 0.92 and 1.38 THz.

a great deal of uncertainty in the data after 1.8 THz; consequently, signals beyond 1.8 THz were not studied. Overall, the refractive index can be used to distinguish the different PGRs.

Each PGR has distinctive characteristics because of its special vibrational modes in the THz region. Fig. 6 shows the absorption spectra of glyphosine, naphthaleneacetic acid,

daminozide, and gibberellic acid at 0.3–1.8 THz. The four PGRs have their own spectral characteristics, including the number and position of absorption peaks.

The four PGRs have obvious absorption peaks from 0.3 to 1.0 THz (Fig. 6(a)). The fingerprint absorption peaks of daminozide at 0.33, 0.39, 0.55, and 0.67 THz are strongest. Although some absorption characteristics are observed at 0.92 THz, the
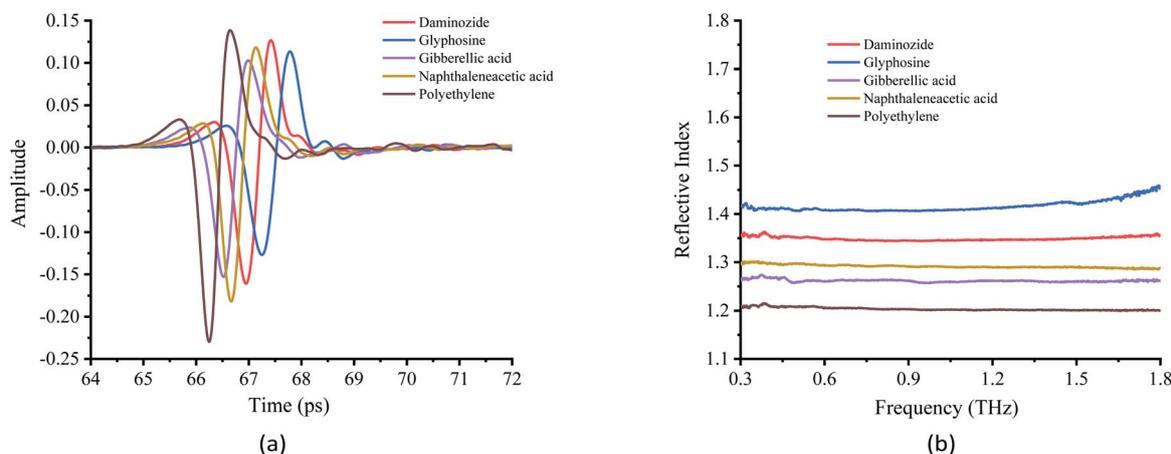

Fig. 5 Terahertz time-domain spectra and terahertz reflective spectra. (a) Terahertz time-domain spectra. (b) Terahertz reflective spectra.
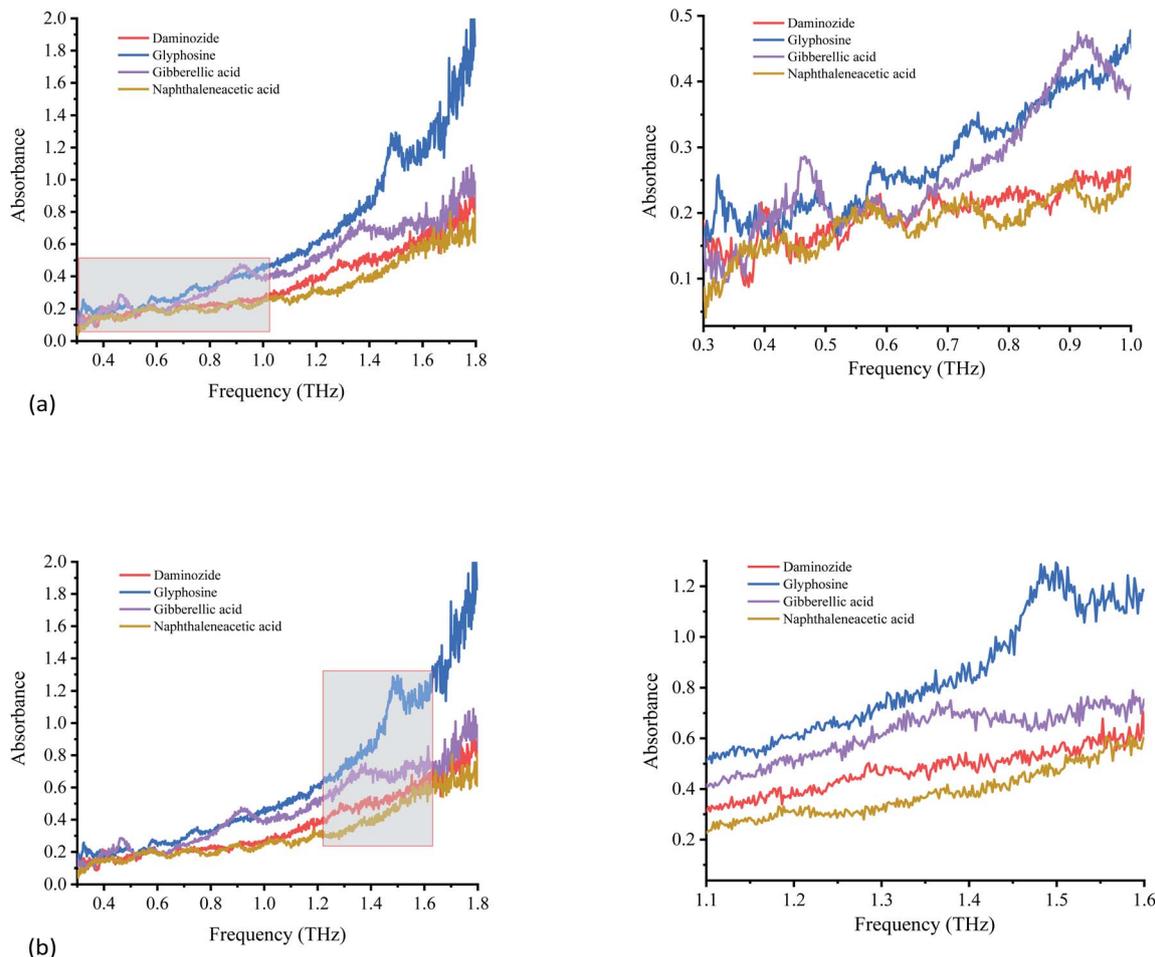
Fig. 6 Variation of absorption coefficients of PGRs. (a) Variation of absorption coefficients of PGRs from 0.3 to 1.0 THz. (b) Variation of absorption coefficients of PGRs from 1.1 to 1.6 THz.

absorption peak is not obvious. The other PGRs can also be discriminated based on the absorption peak positions of glyphosine at 0.32, 0.48, 0.74, and 0.87 THz; gibberellic acid at 0.46, 0.58, and 0.92 THz; and naphthaleneacetic acid at 0.43, 0.55, 0.71, and 0.88 THz.

Fig. 6(b) shows the absorption spectra of glyphosine, naphthaleneacetic acid, daminozide, and gibberellic acid at 1.1–1.6 THz. The absorption characteristics of the four PGRs are not obvious. Only glyphosine has an obvious absorption peak at 1.49 THz. Gibberellic acid exhibits weak absorption characteristics at 1.38 THz. Although the other two PGRs showed no obvious absorption peaks from 1.1 to 1.6 THz, the four PGRs have different absorption characteristics from 1.1 to 1.6 THz. These differences permit these PGRs to be distinguished.

3.3 Quantitative analysis performance

Discriminating among samples based on their spectral features was difficult because of the slight changes in the experimental environment and the similarity of the THz spectra of glyphosine, naphthaleneacetic acid, daminozide, and gibberellic acid samples. We thus used chemometric methods to distinguish

these four PGRs; specifically, we conducted (principal component analysis) PCA on the THz spectra of the four PGRs.[36–38] Because of the fingerprint absorption peaks and the high signal-
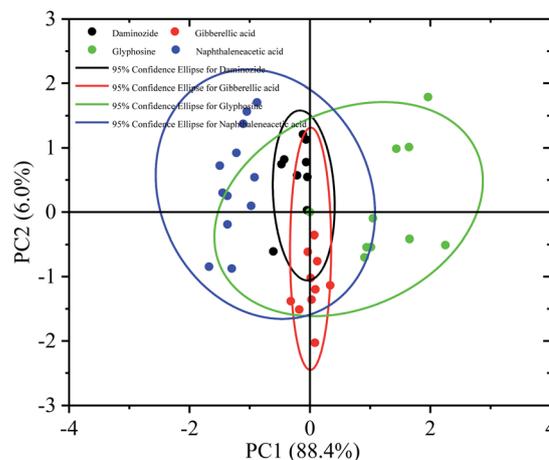

Fig. 7 Score plot of PC1 *vs.* PC2 of a principle component analysis on THz spectra of four plant growth regulators (daminozide, glyphosine, gibberellic acid, naphthaleneacetic acid).
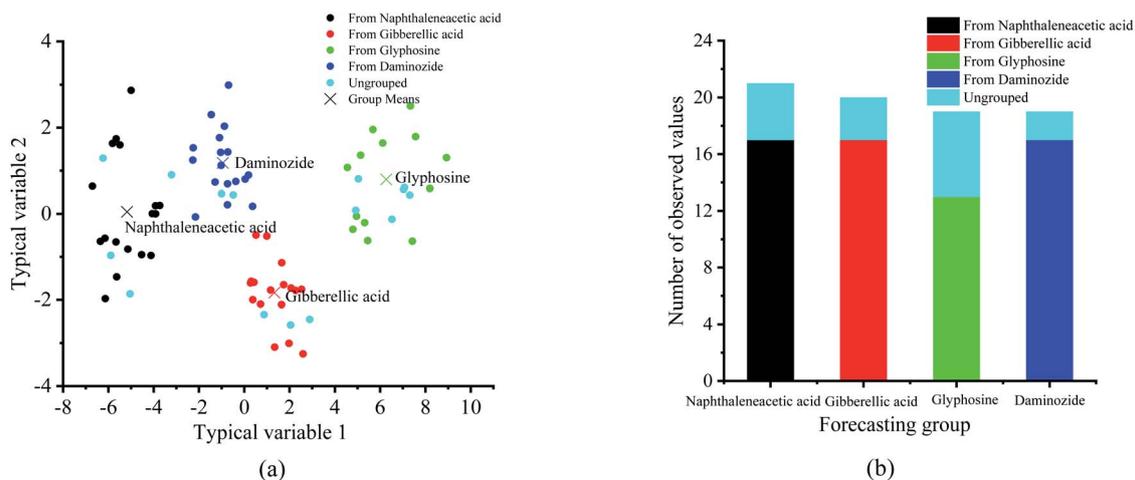
Fig. 8 Classification of four plant growth regulators by using the discriminant analysis method. (a) Typical score chart. (b) Classification summary chart.

to-noise ratio signals, the 1.1–1.3 THz frequency range was used for the quantitative analysis of glyphosine, naphthaleneacetic acid, daminozide, and gibberellic acid (Fig. 7).

A dataset of 80 PGRs samples was used to perform PCA, including 20 samples each of glyphosine, naphthaleneacetic acid, daminozide, and gibberellic acid. Fig. 7 shows the score plot of the principal component scores of the first two principal components (PC1, PC2) for the four PGRs. PC1 and PC2 accounted for 88.4% and 6.0% of the total variance, respectively. Consequently 94.4% as the cumulative variance explained. The four previously defined PGRs (with their corresponding 95% confidence intervals) can be distinguished by PC1 and PC2. Fig. 7 shows that all samples can be clearly distinguished into four categories using the first two PCs. Naphthaleneacetic acid samples are on left of the figure, while glyphosine samples plot on the right side. Gibberellic acid and daminozide samples lie between the two other groups. PCA provides fundamental information on the data structure[39] that can cluster THz absorbance spectra with similar features. However, the difference between the daminozide and the gibberellic acid was not obvious. This result was consistent with the absorption spectrum experimental results in Fig. 6. The main reason may be related to the molecular composition. We can find that the mode causes that the vibration of the daminozide and the gibberellic acid were mainly the vibration between C–H and C–O (Table 1).

In order to further realize the differentiation of four plant growth regulators, the discriminant analysis (DA) method was used to classify the four plant growth regulators samples (Fig. 8). It is different from principal component regression in that it not only decomposes X matrix, but also Y matrix, so as to make the regression result better. In DA, multiple quantitative attributes are applied to determine the variables, which distinguish between two or more naturally occurring clusters. In this study, the 80 samples are divided into four classes (*i.e.* daminozide, glyphosine, gibberellic acid and naphthaleneacetic acid), specifically, 65 samples are used as test samples and 15 samples are used as prediction samples.

Fig. 8(a) shows a plot of the typical score chart of each sample from the four plant growth regulators by using the discriminant analysis method. It can be seen that four PGRs samples were classified correctly in the discriminant analysis model. Meanwhile, the prediction accuracy of this model can achieve 100% (Fig. 8(b)). That is to say, using the discriminant analysis method, the PGRs can be divided to a large extent and a good classification results was obtained.

4. Conclusion

In this study, we obtained the THz spectra of four PGRs at room temperature and analyzed the refractive index and absorption peaks of these PGRs in the 0.3–1.8 THz. DFT was used to analyze the source of each absorption peak. The results showed that the combination of THz-TDS and DFT models with B3LYP/3-21G(*) was effective for characterizing the fingerprint absorption peaks of glyphosine, naphthaleneacetic acid, daminozide, and gibberellic acid. More generally, this study demonstrates the efficacy of using both DFT and THz spectroscopy for the high-performance analysis of biological and chemical molecules. In addition, DA was effective for evaluating the classification trends of the four PGRs by clustering THz absorbance spectra with similar features.

Author contributions

Xuexiao Du: conceptualization, data curation, formal analysis, methodology, software, writing-original draft. Yafei Wang: conceptualization. Xiaodong Zhang: funding acquisition, resources. Guoxin Ma: data curation. Yong Liu: formal analysis. Bin Wang: software. Hanping Mao: funding acquisition, resources, reviewers.

Conflicts of interest

The authors declare that there are no conflicts of interest regarding the publication of this study.

Acknowledgements

References

1 H. Zhang, X. Wu, Y. Yuan, *et al.* An ionic liquid functionalized graphene adsorbent with multiple adsorption mechanisms for pipette-tip solid-phase extraction of auxins in soybean sprouts, *Food Chem.*, 2018, **265**, 290–297.

2 J. Chen, S. Cao, M. Zhu, *et al.* Fabrication of a high selectivity magnetic solid phase extraction adsorbent based on β-cyclodextrin and application for recognition of plant growth regulators, *J. Chromatogr. A*, 2018, **1547**, 1–13.

3 R. Patil, Z. Khan, A. Pudale, A. Shabeer, A. Patil, K. Banerjee, *et al.* Comprehensive multiresidue determination of pesticides and plant growth regulators in grapevine leaves using liquid- and gas chromatography with tandem mass spectrometry, *J. Chromatogr. A*, 2018, **1579**, 73–82.

4 C. Christina Small and D. Degenhardt, Plant growth regulators for enhancing revegetation success in reclamation: A review, *Ecol. Eng.*, 2018, **118**, 43–51.

5 H. Yan, F. Wang, D. Han and G. Yang, Simultaneous determination of four plant hormones in bananas by molecularly imprinted solid-phase extraction coupled with high performance liquid chromatography, *Analyst*, 2012, **137**, 2884–2890.

6 P. C. Pu, S. K. Lin and W. C. Chuang, Modified QuEChERS method for 24 plant growth regulators in grapes using LC-MS/MS, *J. Food Drug Anal.*, 2018, **26**, 637–648.

7 S. H. Hou, X. W. Sun, L. Z. Chen, *et al.* Amino-modified Scholl-coupling mesoporous polymer for online solid-phase extraction of plant growth regulators from bean sprouts, *Food Chem.*, 2020, **321**, 126702.

8 Z. Yilmaz and C. Ismail, Neurotoxic and immunotoxic effects of indole-3-butyric acid on rats at subacute and subchronic exposure, *Neurotoxicology*, 2009, **30**, 382–385.

9 C. J. Wang, C. Y. Ding, Q. W. Wu, *et al.* Molecularly Imprinted Polymers with Dual Template and Bifunctional Monomers for Selective and Simultaneous Solid-Phase Extraction and Gas Chromatographic Determination of Four Plant Growth Regulators in Plant-Derived Tissues and Foods, *Food Anal. Methods*, 2019, **12**, 1160–1169.

10 X. Esparza, E. Moyano and M. T. Galceran, Analysis of chlormequat and mepiquat by hydrophilic interaction chromatography coupled to tandem mass spectrometry in food samples, *J. Chromatogr. A*, 2009, **1216**, 4402–4406.

11 C. Niki and G. B. Maragou, Determination of Ethephon in Pesticide Formulations by Ion Exchange Chromatography with Indirect Spectrophotometric Detection, *Anal. Lett.*, 2020, **53**, 795–806.

12 Q. Lu, J. H. Wu, Q. W. Yu, *et al.* Using pollen grains as novel hydrophilic solid-phase extraction sorbents for the simultaneous determination of 16 plant growth regulators, *J. Chromatogr. A*, 2014, **1367**, 39–1347.

13 C. Suarez-Pantaleon, J. V. Mercader, C. Agullo, *et al.* Hapten synthesis and polyclonal antibody-based Immunoassay development for the analysis of for chlorfenuron in kiwifruit, *J. Agric. Food Chem.*, 2010, **58**, 8502–8511.

14 M. T. Ruggiero and J. A. Zeitler, Resolving the origins of crystalline anharmonicity using terahertz time-domain spectroscopy and *ab initio* simulations, *J. Phys. Chem. B*, 2016, **120**, 11733–11739.

15 X. Yan, M. Yang, Z. Zhang, *et al.* The terahertz electromagnetically induced transparency-like metamaterials for sensitive biosensors in the detection of cancer cells, *Biosens. Bioelectron.*, 2019, **126**, 485–492.

16 J. Y. Qin, L. J. Xie and Y. B. Ying, A high-sensitivity terahertz spectroscopy technology for tetracycline hydrochloride detection using metamaterials, *Food Chem.*, 2016, **211**, 300–305.

17 B. Y. Qin, Z. Li, F. R. Hu, *et al.* Highly Sensitive Detection of Carbendazim by Using Terahertz Time-Domain Spectroscopy Combined With Metamaterial, *IEEE Trans. Terahertz Sci. Technol.*, 2018, **8**, 149–154.

18 X. D. Sun and J. B. Liu, Measurement of Plumpness for Intact Sunflower Seed Using Terahertz Transmittance Imaging, *J. Infrared Millim. Terahertz Waves*, 2020, **41**, 307–321.

19 E. I. Haddad, F. de M. Josette, *et al.* Chemometrics Applied to Quantitative Analysis of Ternary Mixtures by Terahertz Spectroscopy, *Anal. Chem.*, 2014, **86**, 4927–4933.

20 L. J. Xie, C. Wang, M. Chen, *et al.* Temperature-dependent terahertz vibrational spectra of tetracycline and its degradation products, *Spectrochim. Acta, Part A*, 2019, **222**, 117179.

21 G. Q. Wang, J. L. Shen and Y. Jia, Vibrational spectra of ketamine hydrochloride and 3, 4-methylenedioxymethamphetaminein terahertz range, *J. Appl. Phys.*, 2007, **102**, 013106.

22 T. D. Dorney, R. G. Baraniuk and D. M. Mittleman, Material parameter estimation with terahertz time-domain spectroscopy, *J. Opt. Soc. Am.*, 2001, **18**, 1562–1571.

23 L. Duvillaret, F. Garet and J. L. Coutaz, A reliable method for extraction of material parameters in terahertz time-domain spectroscopy, *IEEE J. Sel. Top. Quantum Electron.*, 1996, **2**, 739–746.

24 T. Chen, Q. Zhang, Z. Li, *et al.* Experimental and theoretical investigations of tartaric acid isomers by terahertz spectroscopy and density functional theory, *Spectrochim. Acta, Part A*, 2018, **205**, 312–319.

25 Q. Q. Wang, J. D. Xue, Y. G. Wang, *et al.* Investigation into tautomeric polymorphism of 2-thiobarbituric acid using experimental vibrational spectroscopy combined with DFT theoretical simulation, *Spectrochim. Acta, Part A*, 2018, **204**, 99–104.

26 M. J. Song, F. Yang, L. P. Liu, *et al.* Research on differences between 2-(2′-pyridyl) benzimidazole and 2-(4′-pyridyl) benzimidazole based on terahertz time-domain spectroscopy, *Spectrochim. Acta, Part A*, 2018, **191**, 125–133.

27 H. Fan, M. M. Liu, M. Q. Xie, *et al.* A combined study on the skeletal vibration of aminopyrine by terahertz time-domain spectroscopy and DFT simulation, *Optik*, 2020, **208**, 163913.

28 Z. M. Zhang, Q. Q. Wang, J. D. Xue, *et al.* Vibrational Spectroscopic Investigation into Novel Ternary Eutectic Formed between Pyrazinamide, Fumaric Acid, and Isoniazid, *ACS Omega*, 2020, **5**, 17266–17274.

29 Z. J. Zhu, Ji. B. Zhang, Y. S. Song, *et al.* Broadband terahertz signatures and vibrations of dopamine, *Analyst*, 2020, **145**, 6006–6013.

30 M. E. Zandler and F. D. Souza, The remarkable ability of B3LYP/3-21G(*) calculations to describe geometry, spectral and electrochemical properties of molecular and supramolecular porphyrin–fullerene conjugates, *C. R. Chim.*, 2006, **9**, 960–981.

31 D. Lee, H. Cheon, S.-Y. Jeong, *et al.* Transformation of terahertz vibrational modes of cytosine under hydration, *Sci. Rep.*, 2020, **10**, 17266–17274.

32 Y. M. Wang, Q. Wang, Z. S. Zhao, *et al.* Rapid qualitative and quantitative analysis of chlortetracycline hydrochloride and tetracycline hydrochloride in environmental samples based on terahertz frequency-domain spectroscopy, *Talanta*, 2018, **190**, 284–291.

33 E. Kavitha, N. Sundaraganesan, S. Sebastian, *et al.* Molecular structure, anharmonic vibrational frequencies and NBO analysis of naphthalene acetic acid by density functional theory calculation, *Spectrochim. Acta, Part A*, 2010, **77**, 612–619.

34 Q. Wang and Y. H. Ma, Qualitative and quantitative identification of nitrofen in terahertz region, *Chemom. Intell. Lab. Syst.*, 2013, **127**, 43–48.

35 T. D. Dorney, R. G. Baraniuk and D. M. Mittleman, Material parameter estimation with terahertz time-domain spectroscopy, *J. Opt. Soc. Am.*, 2001, **18**, 1562–1571.

36 T. Chen, Z. Li, X. H. Yin, *et al.* Discrimination of genetically modified sugar beets based on terahertz spectroscopy, *Spectrochim. Acta, Part A*, 2016, **153**, 586–590.

37 H. Y. Gao, H. P. Mao and X. D. Zhang, Determination of lettuce nitrogen content using spectroscopy with efficient wavelength selection and extreme learning machine, *ZEMDIRBYSTE-AGRICULTURE*, 2015, **102**, 51–58.

38 Md. Ashraful Alama, M. Markiewicz-Keszycka, C. Pasquet, C. Gavald, *et al.* Elemental analysis of fish feed by laser-induced breakdown spectroscopy, *Talanta*, 2020, **219**, 121258.

39 N. Yang, X. Zhou, D. F. Yu, *et al.* Pesticide residues identification by impedance time-sequence spectrum of enzyme inhibition on multilayer paper-based microfluidic chip, *J. Food Process Eng.*, 2020, e13544.